Physics of Plasmas ARTICLE scitation.org/journal/php

Generation of high-current pulses by a magnetized squeezed electron beam

Cite as: Phys. Plasmas **26**, 093107 (2019); doi: 10.1063/1.5121484
Submitted: 25 July 2019 · Accepted: 26 August 2019 ·
Published Online: 9 September 2019

J. G. Leopold, Y. P. Bliokh, M. Siman-Tov, and Ya. E. Krasik

AFFILIATIONS

Physics Department, Technion, Israel Institute of Technology, Haifa, Israel

ABSTRACT

The space charge limited current of an electron beam generated in a magnetically insulated foil-less diode by a cylindrical or hollow cathode and injected into a cylindrical drift tube depends on the energy of the electrons and on the ratio of the beam radius to the tube radius. When this beam drifts into a tube of larger radius, it exceeds the corresponding space charge limit. This leads to the formation of a virtual cathode and to the reduction of the energy of the beam. The latter is known as a squeezed beam state. When the cylindrical tube consists of more segments of different radii and lengths, the dynamics of the beam can be manipulated. We propose a simple configuration resulting in the production of a high-frequency periodic train of high-current electron beam pulses.

I. INTRODUCTION

A large number of publications, in particular from the former Soviet Union since the 1970s[1] and up to recently, deal with the propagation of high-current electron beams in nonuniform conducting cylindrical structures. In all these studies, the beam is considered to be strongly magnetized by an external guiding magnetic field. For an electron beam of radius r_b injected into an infinitely long tube of radius R, the amplitude of the current is restricted to its space charge limited value I_{SCL},[1]

$$I_{SCL} = \frac{mc^3}{e}\frac{\left(\gamma^{2/3}-1\right)^{3/2}}{\kappa}. \tag{1}$$

Here, $\frac{mc^3}{e} \approx 17$ kA is the Alfvén current and $\gamma = 1 + \frac{eV}{mc^2}$ is the relativistic factor, where V is the anode potential and κ is the geometrical factor which is given as

$$\kappa_a = 2ln\frac{R}{r_b} \quad \text{and} \quad \kappa_s = 1 + 2ln\frac{R}{r_b}, \tag{2}$$

where a and s stand for the thin walled annular or solid beams, respectively. It is assumed that the tube is much longer than its radius $L \gg R$, the external magnetic field, B_0, is significantly larger than the self-magnetic field produced by the beam current, and the electron Larmor radius is smaller than the beam radius or thickness.[2] For a thin walled (the wall thickness significantly smaller than the beam radius) relativistic annular beam propagating in an infinite tube, it was shown[3] that the space-charge limited current reduces to the asymptotic value, $I_F < I_{SCL}$,

$$I_F = \frac{mc^3}{2eln\frac{R}{r_b}}(\gamma-\gamma_F)\frac{\left(\gamma_F^2-1\right)^{1/2}}{\gamma_F}, \tag{3}$$

where $\gamma_F = (2\gamma + \frac{1}{4})^{1/2} - \frac{1}{2}$. When an electron beam with a current I_0 larger than I_{SCL} (of either form above) is injected into a tube, the current flow is perturbed by the local space charge forces. This leads to a decrease in the electron velocity, and part of the electrons are reflected from a virtual cathode (VC) region. The rest of the beam with current, $I \le I_{SCL}$, flows downstream from this location. When an annular electron beam propagating in a tube carries a current satisfying the condition $I \le I_F$ and flows directly into a tube of larger radius, then this second tube is necessarily "overinjected" because for this tube, $I \ge I_F$ and a VC forms. The excess of the injected current at that location above I_F forms a return current traveling backward toward the injection plane. Along the distance between the VC and the injection plane, the forward and backward currents accumulate charge which may become too large. Then, the repulsive Coulomb force slows the electrons down, and so overall, less charge travels in both directions and less charge is accumulated. This was named by Ignatov and Tarakanov,[5] a *squeezed state* of a high current beam. In Ref. 6, the dynamics of structures with one or two radius transitions were numerically simulated and analyzed.

This fascinating dynamical structure was recently picked up again, and it was suggested that it may be utilized in high-current and high-power microwave devices. Fuks *et al.*[7] considered a magnetically insulated structure with two consecutive sections of increasing radius as the underlying structure of a magnetron with a diffraction output

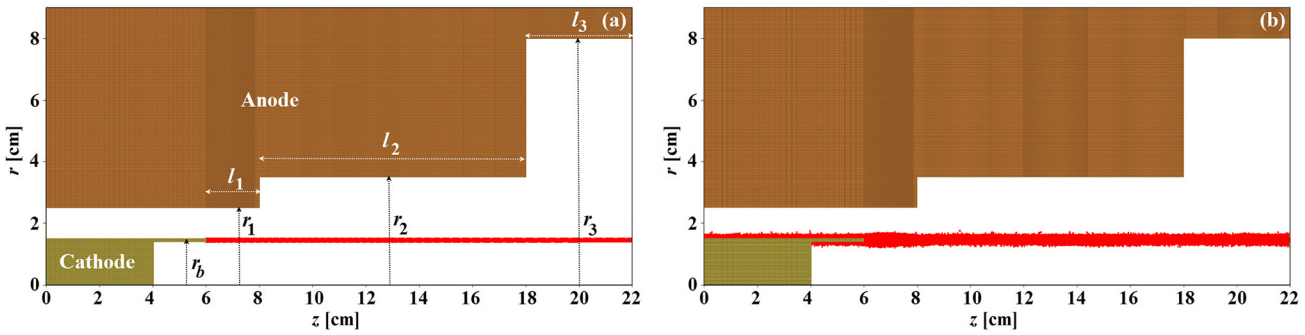

FIG. 1. The PIC simulated electron beam (red dots) at $t = 2$ ns (a) and 80 ns (b) in the $[r, z]$ plane for a three section anode tube of radii 2.5, 3.5, and 8 cm and $l_1 = 2$, $l_2 = 10$, and $l_3 = 4$ cm.

(MDO) where the squeezed charge is used as the magnetron electron source. Gromov *et al.*[8] and Fuks and Schamiloglu[9] have replaced the constant magnetic field with an increasing one, which forms a magnetic mirror forcing the beam exiting the squeezed state region to return to the interaction region of the MDO.

Dubinov *et al.*[10] have shown a variation of these ideas which may be used as a vircator but with a magnetically insulated beam propagating through a long dielectric tube to vacuum. In experiments, Belomyttsev *et al.* added a drift tube consisting of two and three increasing radius cylinders to a magnetically insulated diode of a 2 MV electron accelerator producing a 20 kA, 50 ns long electron beam generated by an annular cathode. It was shown that the current is limited as expected [Eq. (3)], and the existence of the squeezed state was experimentally verified.

Recently, a large amount of work has been invested in the attempt to use the electron plasma density oscillations formed in the squeezed state as a microwave radiation source.[9–13] Our recent work on overinjecting a diode and the development of self-oscillations[14,15] has triggered our interest in studying such high-current electron beam instabilities in an attempt to produce space-charge self-oscillations, resulting in bunched electron beams at the output of the system. In our original scheme,[14] the initial injected current is required to be below the SCL of the voltage gap. The latter can be realized with a thermionic emitter operating in a current limited emission mode (up to a few Amperes). However, such a scheme is impractical for high-current (hundreds to thousands of Amperes) electron beam bunches.

In the present paper, we propose a way to exploit such systems for high-current applications by delaying the formation of the *squeezed state* of a high-current beam and obtain high-current electron bunches during the self-oscillatory period of the oscillating electron beam space charge. Such electron bunches can be used in separate slow wave structures to extract microwave energy, in accelerators or other important applications.[16] We consider here annular beams only though solid beams behave in a similar way. We use the MAGIC PIC (Particle In Cell) code in our simulations.[17]

II. A SYSTEM WITH CONSECUTIVELY INCREASING RADIUS ANODE TUBE SEGMENTS

We first study a diode injecting an annular beam from its hollow thin wall cathode into two consecutive sections with increasing radii (Fig. 1). In the 3D-PIC simulations in cylindrical coordinates, we assume that only the 1 mm thick tip of the hollow $r_b = 1.5$ cm radius cathode emits a space-charge-limited current. A uniform 2 T axial magnetic field is present in all our calculations. The three consecutive anode tube segments of radii $r_1 = 2.5$ cm, $r_2 = 3.5$ cm, and $r_3 = 8$ cm are $l_1 = 2$ cm, $l_2 = 10$ cm, and $l_3 = 4$ cm long. A 150 kV voltage pulse rising in 1 ns is applied at $z = 0$ from which it advances as a TEM wave into the system and from which it exits at $z = 22$ cm (Fig. 1).

In Fig. 2, the time dependence of the input voltage, the emitted current, the current collected on the downstream boundary, and the upstream current, that is, the current collected on the upstream boundary and the nonemitting cathode surfaces [see Fig. 1(b)], is drawn.

The behavior of the PIC calculated values of the input voltage and various currents in Fig. 2 can be understood by studying the time dependent electron dynamics in the $[p_z, z]$ phase-space displayed in Fig. 3. In Fig. 3(a) at $t = 2.1$ ns, the beam has just reached the downstream boundary. At $t = 4.0$ ns [Fig. 3(b)], near the two radial increase points, VCs develop. In Fig. 3(c) ($t = 5.8$ ns), return currents from the two VCs are seen and the return current from the first VC has just reached the emitter. This coincides with the reduction of the emitted current in Fig. 2. The MAGIC-PIC code treats the input boundary as an electromagnetic incoming wave, displaying a voltage difference between the coaxial cathode and anode. This assumes an impedance which depends at first on the cathode anode distance. As the wave

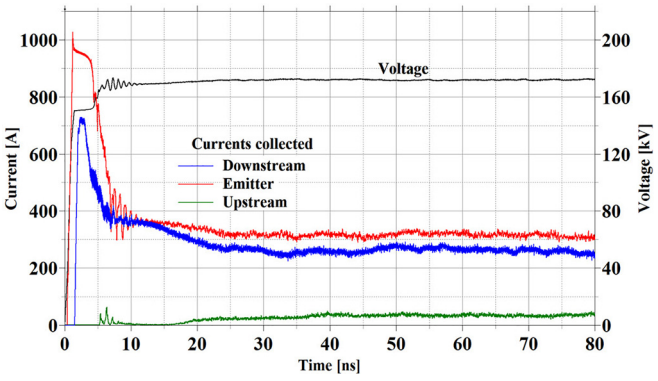

FIG. 2. The input voltage (black) and the emitted (red), the downstream (blue), and the upstream (green) currents vs time for the case seen in Fig. 1.

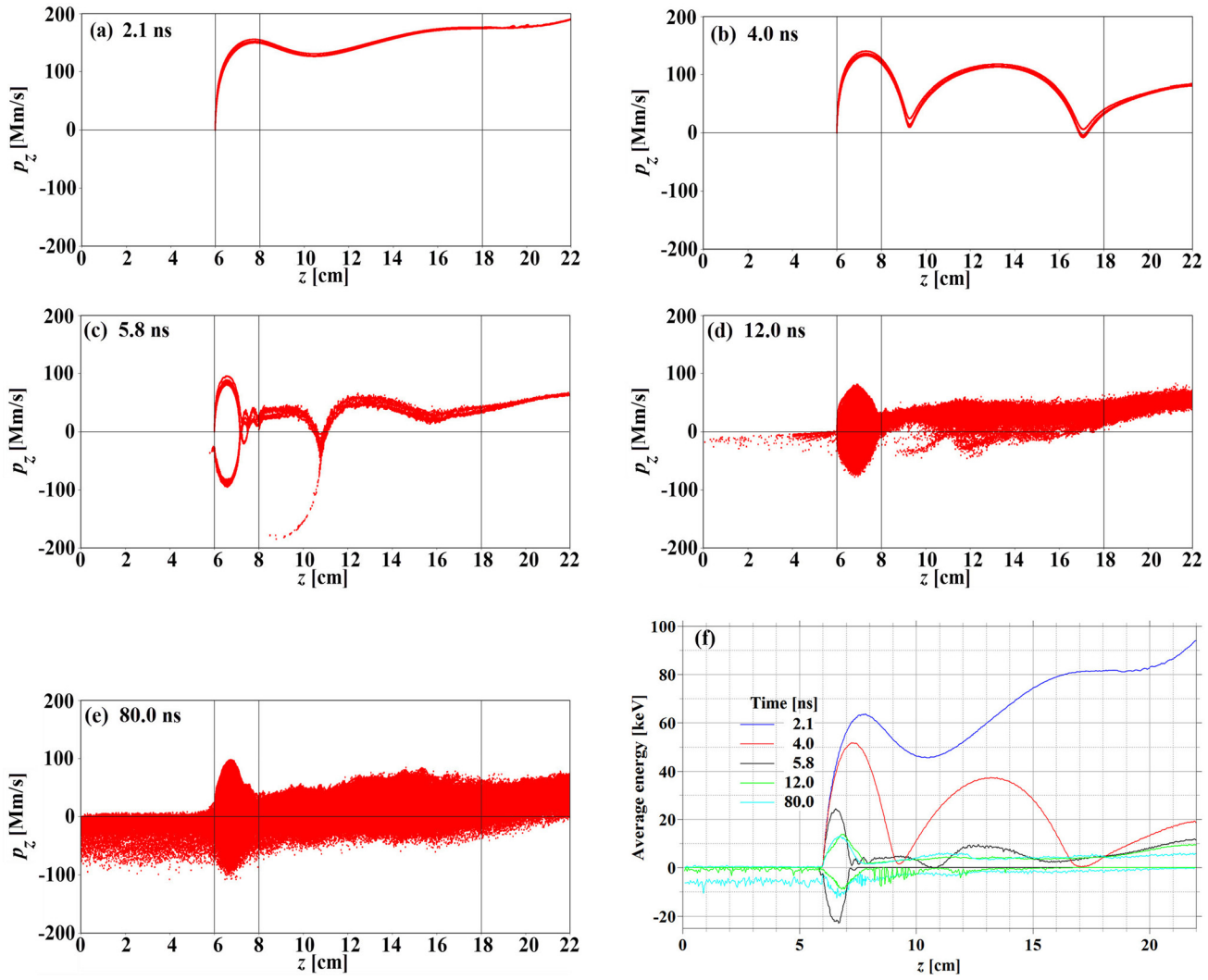

FIG. 3. PIC simulated [p_z,z] phase-space snapshots at 2.1 (a), 4.0 (b), 5.8 (c), 12.0 (d), and 80 ns (e) for the three segment system in Fig. 1. Grid lines are drawn at the position of the emitter tip and the two radial transition points. (f) The average energy vs z at the same points in time as in (a)–(e). The average energy of downstream flowing electrons (positive energy lines) is displayed separately from electrons flowing upstream (negative energy lines).

propagates and the emitted current reduces because of the formation of the VCs and the increasing return current, the voltage needs to increase because of the increased diode impedance.

After ∼4 ns, the voltage increases from 150 kV to ∼172 kV, while the emitted current decreases from ∼960 A to ∼360 A. I_{SCL} values calculated using Eq. (3) for $R = r_1$ and r_3 are 970 A (150 kV) and 360 A (172 kV), respectively, which agree with these PIC calculated results. This lower value holds up to ∼12 ns when both the emitter and downstream currents reduce further to a level of ∼310 and ∼260 A, respectively, during the next 15–25 ns, while the voltage further increases slightly. At the same time, a current appears on the upstream boundary and the nonemitting surfaces of the cathode. The appearance of this current is the result of the increasing beam width [see Fig. 1(b)] and its upstream flow away from the emitter [Fig. 3(d)]. Note the small oscillations mainly in the emitted current and the voltage before the beam reaches a steady state flow and the corresponding small turbulences at z ∼ 7–8 cm as seen in Fig. 3(c). In time, the system settles to a steady phase space distribution as that seen in Fig. 3(e).

In Fig. 3(f), the average electron energies of the downstream flowing electrons and the upstream flowing electrons are drawn separately as positive and negative values, respectively, at the time instants as those of the snapshots in Figs. 3(a)–3(e). There is no negative flow for $t \leq 5.8$ ns, but since too much space charge accumulates in the upstream larger radius segment, first, the beam energy reduces below the accelerating energy followed by the formation of two VCs. In Fig. 4, we draw curves along the top of the histogram of the number of electrons along the beam in longitudinal bins of $\Delta z = 2$ mm containing Δn electrons. Below this value of Δz, these curves do not change and they represent a longitudinal electron density $\Delta n/\Delta z$ for this thin annular beam. In time, the energy of the electrons reduces

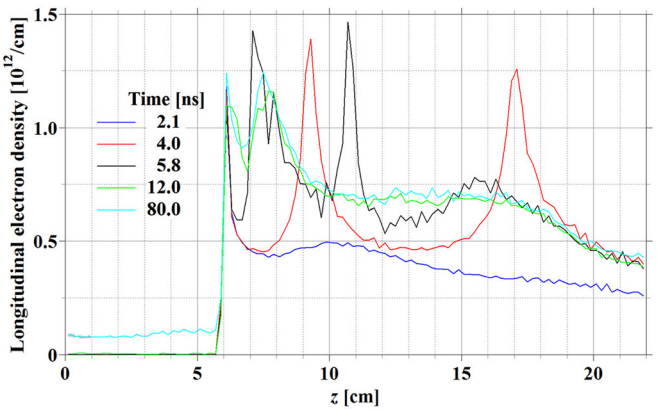

FIG. 4. The longitudinal electron density along the beam of Fig. 1 at the same times as in Fig. 3(f).

considerably to a steady low energy flow as the *squeezed state* is reached as soon as 12 ns [Fig. 3(f) and the beam density increases along the central region of the three segment tube (Fig. 4) where the electrons move slowly down- and up-stream [Fig. 3(f)].

Most of the dynamics presented in this section has been observed in the early literature,[4,6] but its present analysis will be useful to understand and compare the results of the manipulations introduced in Secs. III and IV.

III. DELAYING THE FORMATION OF A SQUEEZED STATE

The anode radial transitions following the magnetically insulated foil-less coaxial diode is a system where VCs form by design. The presence of more than a single VC along an axial distance can cause oscillatory electron motion between the VCs. For systems such as that studied in Sec. II, the electron oscillations are suppressed during the first few nanoseconds due to the electron distribution function's spread in the phase space and the formation of the squeezed beam state [see Figs. 3(d) and 3(e)]. The main purpose in this work is to delay the formation of the squeezed state and design the system to oscillate and release periodic high-current electron bunches.

There are two sources of the electrons dispersing in phase space. First, electrons reflected from the oscillating VC are not monoenergetic, and this energy spread destroys the coherent structure of the particles' flux. This inherent property of the VC cannot be eliminated. The second reason is the repulsive Coulomb force of the space charge which moves electrons away from each other and decreases the spatial modulation of the electron density permanently. This effect, in principle, can be considerably weakened.

The difference between the beam and SCL currents is the measure of the effect of space charge on the electron motion: the larger the difference between the two, the smaller the Coulomb repulsion force. Thus, the space charge repulsive forces which damp the current modulation can be reduced if the radius of the second section is smaller than the radii of the first and the third sections, so that $I < I_{SCL}$. The Coulomb force will manifest itself when the space charge accumulated in this section becomes large enough. The larger the ratio I_{SCL}/I, the longer the time required for the accumulation of this amount of charge and the longer the duration of the current oscillations.

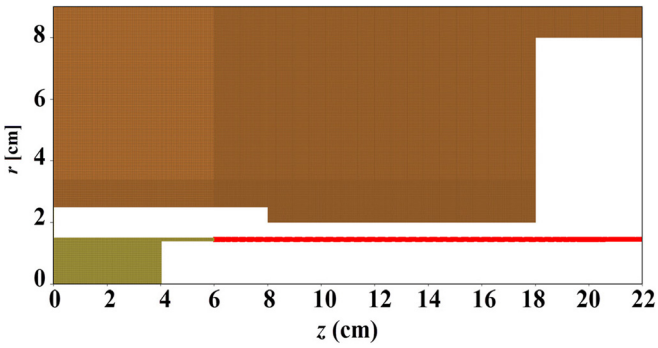

FIG. 5. The PIC simulated position of the electron beam (red dots) at $t = 2$ ns for a system of 3 segments of radii 2.5, 2, and 8 cm and $l_1 = 2$, $l_2 = 10$, and $l_3 = 4$ cm.

Here, let us note that in Ref. 11, an anode segment of smaller radius than that of the anode tube of the coaxial diode segment has been introduced as an *anode insert*. Other than using this midsection's distance from the emitter to control the emitted current, its dynamical role was not studied.

We consider the geometry of the system seen in Fig. 5 which differs from that studied in Sec. II in that the midsegment has a smaller radius ($r_2 = 2.0$ cm) than the upstream segment ($r_1 = 2.5$ cm).

In Fig. 6, the PIC calculated time dependence of the voltage at the upstream boundary and currents at various points along the system is displayed.

The only difference between the cases studied in Figs. 6 and 2 is in the radius of the midsegment, $r_2 = 2.0$ cm and 3.5 cm, respectively. At the same time, the behavior of the currents is very different. The voltage increases and the emitted current decreases at ~4 ns for both cases, which reflects the return current's arrival to the cathode. From this point for the larger radius midsegment, the voltage and the currents stabilize, whereas for $r_2 < r_1 < r_3$, all oscillate for a period of a few tens of nanoseconds. The reason for this is explained next.

In Fig. 7, the electron phase space is displayed for time instants which represent the main features of the dynamics.

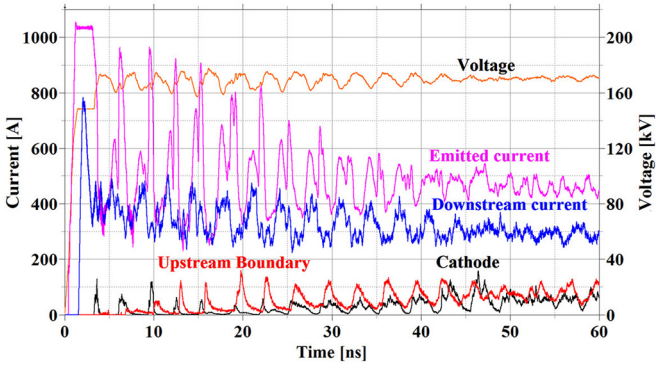

FIG. 6. Time dependence of the voltage at the upstream boundary, the emitted current (violet), the current crossing the downstream boundary (blue), the current crossing the upstream boundary (red), and the current collected on the nonemitting cathode surfaces (black) for the system in Fig. 5.

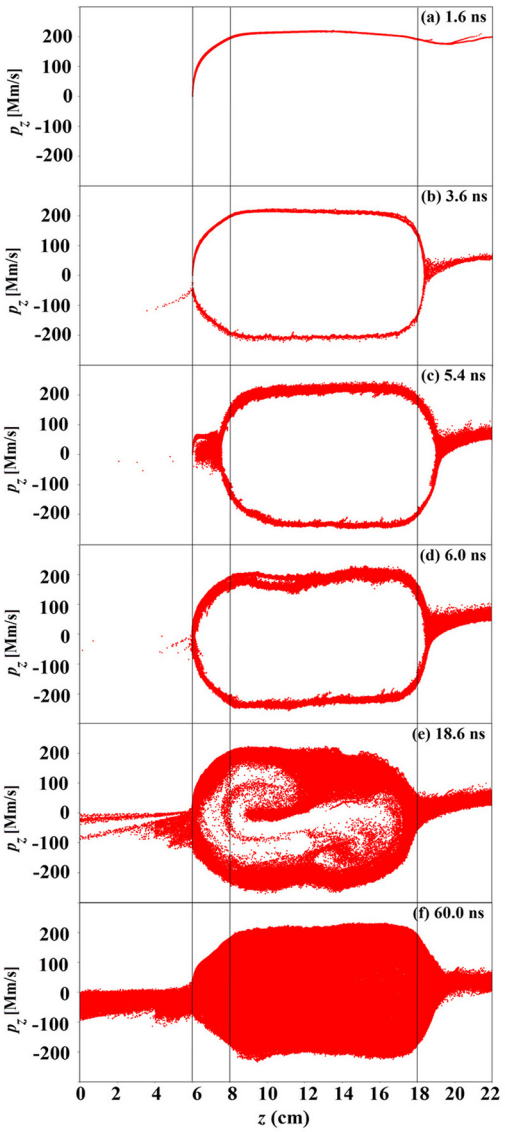

FIG. 7. PIC simulated [p_z,z] phase-space snapshots at 1.6 (a), 3.6 (b), 5.4 (c), 6.0 (d), 18.6 (e), and 60 ns (f) for the system of Fig. 5. The vertical gridlines at $z = 6$, 8, and 18 cm point out the position of the emitter, the r_1-r_2 transition point, and the r_2-r_3 transition point, respectively.

In contrast to Fig. 3, the VC at the r_2-r_3 transition does not disappear while squeezing turns on. The VC near the emitter moves between the emitting point and the position of the r_1-r_2 transition point [Figs.7(b)–7(d)]. This is responsible for the oscillation in the emitted current as seen in Fig. 6 at a frequency of ∼290 MHz of the order of a round trip between the VCs. At the same time, the r_2-r_3 VC counter reacts with similar oscillations responsible for the appearance of (weaker) oscillations in the current exiting the system downstream. In time, the phase space island fills up rather than squeezing completely [compare Figs. 7(e)–7(f) with 3(d)–3(e)]. At first, turbulent flow develops with periodic structures [Fig. 7(e)]; at later times, the island fills up completely, its size remains the same, and the VC oscillations in z are less apparent.

In Fig. 8, the average electron energies corresponding to Figs. 7(a) and 7(e)–7(f) are displayed. In contrast to Fig. 3(f), it is clear that though squeezing is attempting to set in along the island, the process is delayed significantly, and at the same time, the average energy of the electrons does not decrease to the several kilo-electron-volt level as seen in Fig. 3(f).

Finally, in Fig. 9, we observe that later in the process, the beam becomes unstable in the radial direction. The beam disperses in r nonuniformly, in spite of the presence of the strong axial magnetic field, and negligible charge is shed to the anode up to the times considered here. We have performed calculations by increasing the axial magnetic field up to 10 T with very little effect. The forces ($\boldsymbol{E}_r \times \boldsymbol{B}_z$) within the space charge accumulating in the midsection also produce fast azimuthal electron motion which decreases the external magnetic field locally because it consists of a diamagnetic current. In Fig. 10, this azimuthal flow can be discerned with off-annular charge rotating around the axis. This azimuthally nonuniform space charge can lead to radial $\boldsymbol{E}_\theta \times \boldsymbol{B}_z$ drift of electrons toward the anode. This very interesting unstable radial motion of the beam will be analyzed in more detail in the future.

Thus, we have confirmed that the existence of a midsegment of lower radius, which can accommodate a higher charge than elsewhere, delays squeezing and allows an oscillatory behavior over a considerable time. The quality of the oscillations of the current at the downstream boundary is not though sufficient for producing electron bunches.

IV. IMPROVING THE OSCILLATORY BEHAVIOR

To improve the oscillatory behavior, we add an electrode at a distance of 1 cm downstream from the structure studied in Sec. III as seen in Fig. 11.

A voltage difference $V_1 = 150$ kV between the cathode and the anode is applied at the upstream boundary which increases to 180 kV as before. A second decelerating negative voltage difference of $V_2 = -180$ kV is applied between the anode and the additional electrode (Fig. 11). The rationale for adding a third electrode is that by decelerating the electrons in addition to the natural slow down at the

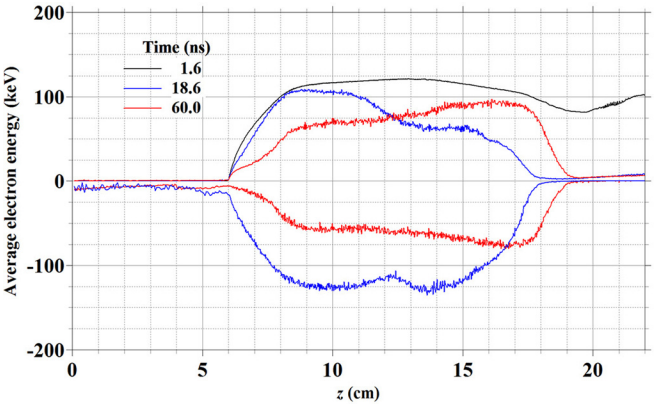

FIG. 8. The average energy of the downstream (positive values) and upstream (negative values) flowing electrons at 1.6 (black), 18.6 (blue), and 60 ns (red).

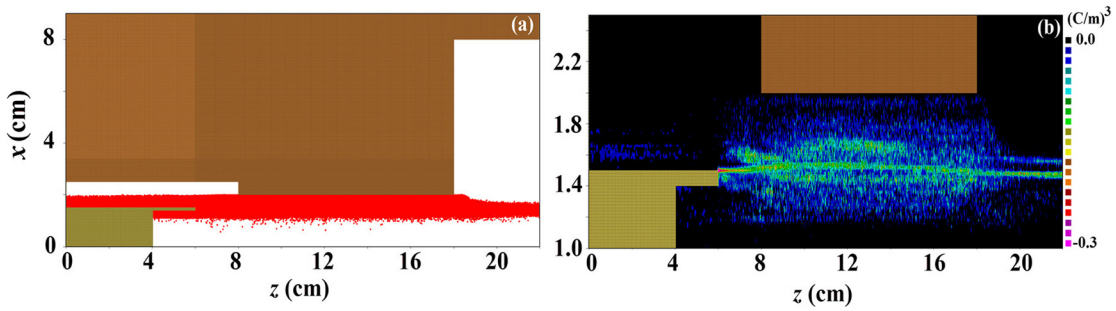

FIG. 9. (a) The beam position in an [x,z] plane and (b) the electron charge distribution in the same plane but the magnified, at t= 57.4 ns.

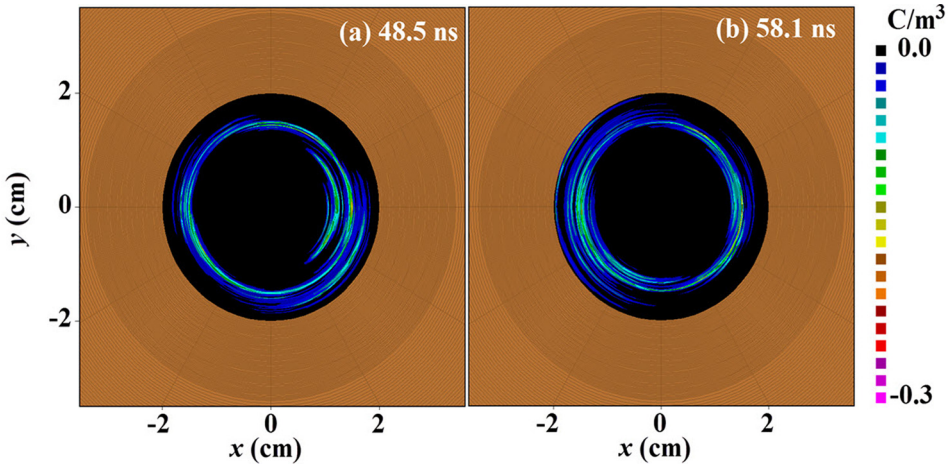

FIG. 10. The electron charge distribution in the [x,y] plane at z = 13 cm at the center of the midsection at (a) t = 48.5 ns and (b) 58.1 ns.

VC, even more charge is forced into the midsegment of the anode. As $|V_2|$ is increased, the electron bunches become more and more pronounced, and at 180 kV, the current detaches from the electrode (zero collected current) periodically between the appearance of two bunches. A further increase in $|V_2|$ stops the current from arriving to this electrode altogether. The results for $V_2 = -180$ kV are seen in Fig. 12.

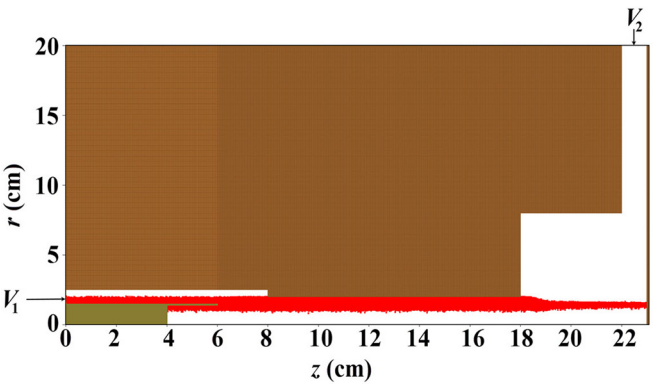

FIG. 11. The same structure as that in Fig. 9(a) with an additional electrode at z = 23 cm. The electron beam is seen here for V_1 = 150 kV and V_2 = −180 kV at 70 ns.

The behavior of the other currents and the phase space are similar to the case without the decelerating electrode, and the current shed to the anode during the calculated time remains negligible. The results in Fig. 12 show that the addition of this electrode

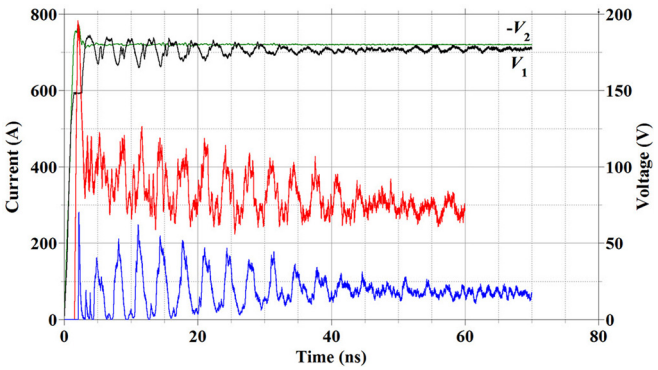

FIG. 12. The time dependence of the voltage applied on the upstream boundary, V_1 (black), the negative value of V_2 (green), and the current collected on the downstream electrode (blue). For comparison, the current at the downstream boundary in the absence of the additional decelerating electrode (from Fig. 6) is also drawn (red).

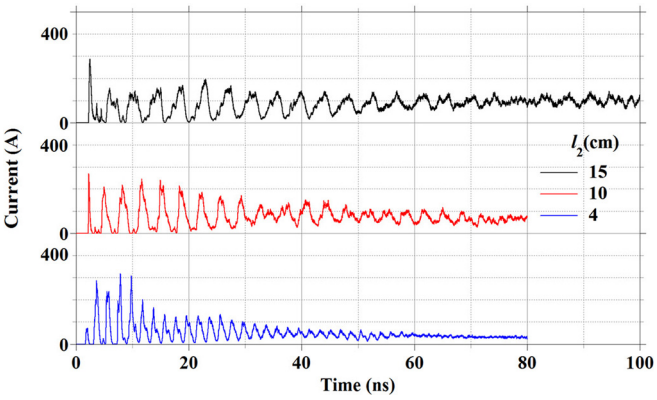

FIG. 13. The time dependence of the current collected on the downstream electrode for different values of l_2.

forces the background current which flows downstream without being slowed down from a level of ∼250 A (red curve in Fig. 12) to ∼90 A (the blue curve in Fig. 12) and ∼1.5 ns long [at full width half maximum (FWHM)] electron bunches appear during the first ∼30–40 ns carrying ∼150–200 A which are collected on the additional electrode with the same frequency as the oscillations seen before. We have calculated the effect of increasing the value of the voltage difference $|V_2|$ and found that we need 180 kV at the top of the increased value of V_1 (Fig. 12) to best separate between the electron bunches. The oscillation period is of the order of the round trip of the beam between the two VCs along the midsegment. To test this, we study the effect of varying the length, l_2, of the midsegment (Fig. 13). As the length of the midsection increases, the bunch current maxima decrease, the time over which oscillations occur increases, and the bunch appearance frequency decreases (501, 293, and 232 MHz for $l_2 = 4$, 10, and 15 cm, respectively). This is additional proof for the fact that the bunch formation frequency is related to the round trip transit time, i.e., the temporal build-up and collapse of the VCs due to subsequent depression of the electron emission from the cathode by the oscillating space charge of electrons.

If the downstream electrode is replaced by a fairly transparent grid, the electron bunches exit the system and can be used in any chosen application.

V. CONCLUSIONS

Simulation results confirm our idea that by introducing after the coaxial diode segment a midsection with a radius smaller than the radius of the diode anode, followed by a larger radius anode segment of a cylindrical electron beam system immersed in a strong magnetic field, it is possible to make the system self-oscillate for a considerable time before squeezing takes over. These self-oscillations can produce a train of high current bunches appearing at a frequency which depends on the round trip time of electrons between the VC near the cathode and that near the second radius transition.

In this paper, we have chosen the lengths of the various sections qualitatively. The length of the cathode segment was chosen so that the cathode is sufficiently far away from the upstream boundary so that the electromagnetic wave's propagation in the coaxial tube section has only a small effect on the particle dynamics. The distance between the cathode emitting surface and the first anode radius change affects the emitted current for a given voltage. The length of the midsection affects the oscillation frequency and amplitude, but it is limited. If too short, squeezing can turn on before oscillations develop as the two VCs overlap; if too long, the two VCs may be too far apart; downstream and upstream current flows constantly, and all excess charge is contained so that no charge bursts exit the downstream VC and squeezing is delayed for a very long time. The length of the third segment was chosen so that the beam is collected close to the exit point from the second virtual cathode.

The frequency range of the oscillatory behavior in the present paper is in the range of 232–501 MHz, which may be too low for microwave applications. The upper limit of the oscillating frequency should depend not only on the geometry but also on the electron energy and current. This is the next step in our research where we shall use analysis and simulations to test this issue.

The dynamics of this highly nonlinear system is extremely complicated, but its potential is far from being harvested.

REFERENCES

[1]B. N. Brejzman and D. D. Ryutov, Nucl. Fusion **14**, 873 (1974).
[2]L. S. Bogdankevich and A. A. Rukhadze, Sov. Phys.-Usp. **14**, 163 (1971).
[3]A. I. Fedosov, E. A. Litvinov, S. Y. Belomytsev, and S. P. Bugaev, Sov. Phys. J. **20**, 1367 (1977).
[4]N. F. Kovalev, Tech. Phys. **47**, 906 (2002).
[5]A. M. Ignatov and V. P. Tarakanov, Phys. Plasmas **1**, 741 (1994).
[6]A. E. Dubinov and I. A. Efimova, Tech. Phys. **46**, 723 (2001).
[7]M. I. Fuks, S. Prasad, and E. Schamiloglu, IEEE-Trans. Plasma Sci. **44**, 1298 (2016).
[8]A. V. Gromov, M. B. Goykhman, N. F. Kovalev, A. V. Palitsin, M. I. Fuks, and E. Schamiloglu, Tech. Phys. Lett. **44**(10), 949 (2018) [Pis'ma Zh. Tekh. Fiz. **44**(20), 102 (2018)].
[9]M. I. Fuks and E. Schamiloglu, Phys. Rev. Lett. **122**, 224801 (2019).
[10]A. E. Dubinov, A. G. Petrik, S. A. Kurkin, N. S. Frolov, A. E. Koronovskii, and A. E. Hramov, Phys. Plasmas **24**, 073102 (2017).
[11]S. Ya. Belomyttsev, A. A. Grishkov, S. A. Kitsanov, S. D. Korovin, S. D. Polevin, and V. V. Ryzhov, Tech. Phys. Lett. **31**, 55 (2005); S. Ya. Belomyttsev, A. A. Grishkov, S. A. Kitsanov, S. D. Korovin, S. D. Polevin, V. V. Ryzhov, and A. P. Yachnyi, *ibid.* **31**, 982 (2005); S. Ya. Belomyttsev, A. A. Grishkov, S. A. Kitsanov, I. K. Kurkan, S. D. Polevin, V. V. Ryzhov, and R. V. Tsygankov, *ibid.* **34**, 546 (2008); **37**, 128 (2011).
[12]A. G. Petrik, S. A. Kurkin, A. A. Koronovskii, and A. E. Hramov, Tech. Phys. Lett. **42**, 792 (2016).
[13]A. E. Dubinov, A. G. Petrik, S. A. Kurkin, N. S. Frolov, A. E. Koronovskii, and A. E. Hramov, Phys. Plasmas **24**, 042105 (2016).
[14]J. G. Leopold, M. Siman-Tov, A. Goldman, and Y. E. Krasik, Phys. Plasmas **24**, 073116 (2017).
[15]M. Siman-Tov, J. G. Leopold, and Y. E. Krasik, Phys. Plasmas **26**, 033113 (2019).
[16]A. Pedersen, A. Manolescu, and A. Valfells, Phys. Rev. Lett. **104**, 175002 (2010).
[17]B. Goplen, L. Ludeking, D. Smith, and D. Warren, "User configurable MAGIC for electromagnetic PIC calculations," Comput. Phys. Commun. **87**, 54 (1995).